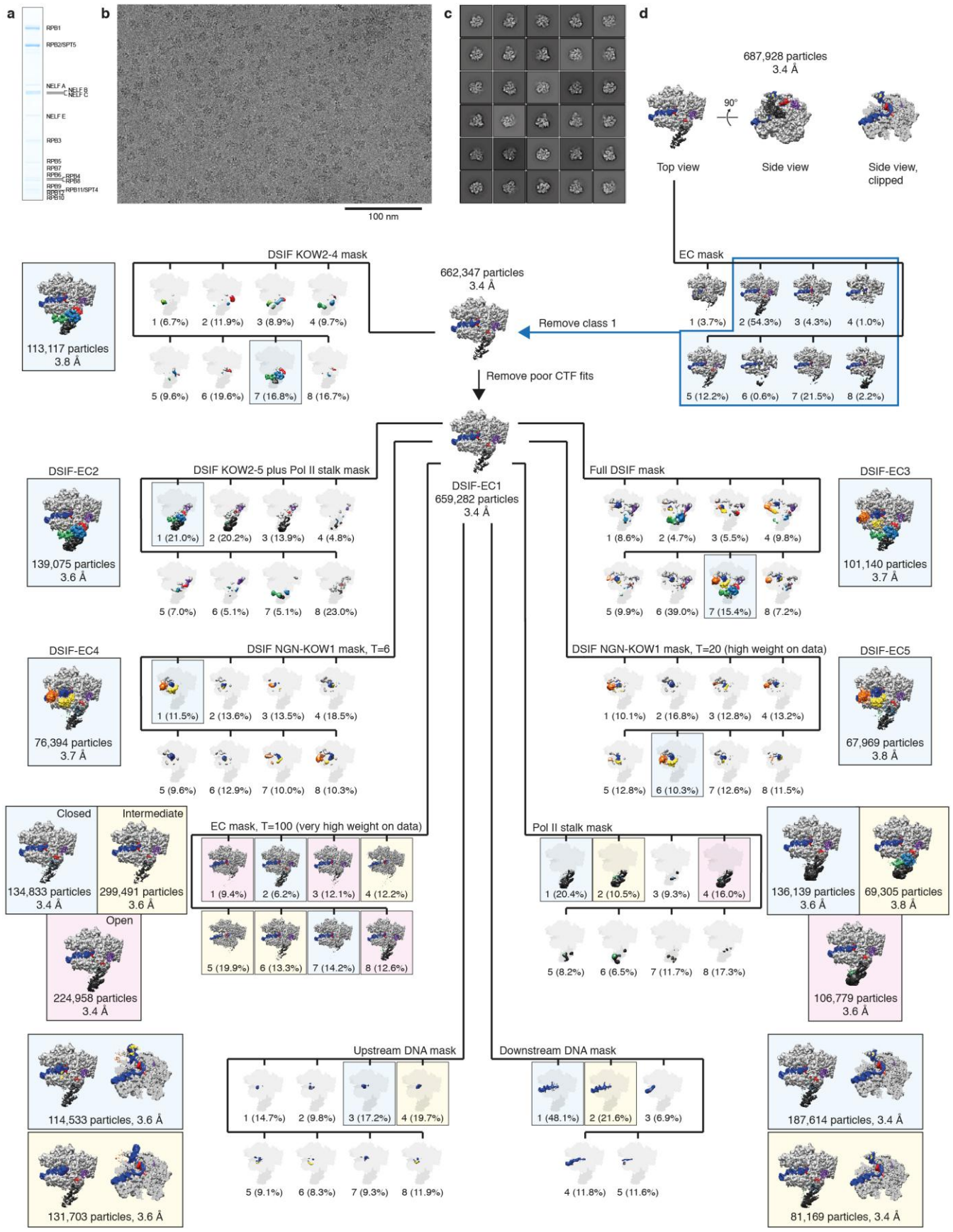
a
RPB1
RPB2/SPT5
NELF A
NELF B
NELF C
NELF E
RPB3
RPB5
RPB7
RPB6
RPB4
RPB8
RPB9
RPB12
RPB10
RPB11/SPT4
b
100 nm
c
d
687,928 particles
3.4 Å
90°
Top view
Side view
Side view, clipped
EC mask
1 (3.7%)
2 (54.3%)
3 (4.3%)
4 (1.0%)
5 (12.2%)
6 (0.6%)
7 (21.5%)
8 (2.2%)
Remove class 1
662,347 particles
3.4 Å
DSIF KOW2-4 mask
1 (6.7%)
2 (11.9%)
3 (8.9%)
4 (9.7%)
5 (9.6%)
6 (19.6%)
7 (16.8%)
8 (16.7%)
113,117 particles
3.8 Å
Remove poor CTF fits
DSIF-EC1
659,282 particles
3.4 Å
DSIF-EC2
139,075 particles
3.6 Å
DSIF KOW2-5 plus Pol II stalk mask
1 (21.0%)
2 (20.2%)
3 (13.9%)
4 (4.8%)
5 (7.0%)
6 (5.1%)
7 (5.1%)
8 (23.0%)
Full DSIF mask
1 (8.6%)
2 (4.7%)
3 (5.5%)
4 (9.8%)
5 (9.9%)
6 (39.0%)
7 (15.4%)
8 (7.2%)
DSIF-EC3
101,140 particles
3.7 Å
DSIF-EC4
76,394 particles
3.7 Å
DSIF NGN-KOW1 mask, T=6
1 (11.5%)
2 (13.6%)
3 (13.5%)
4 (18.5%)
5 (9.6%)
6 (12.9%)
7 (10.0%)
8 (10.3%)
DSIF NGN-KOW1 mask, T=20 (high weight on data)
1 (10.1%)
2 (16.8%)
3 (12.8%)
4 (13.2%)
5 (12.8%)
6 (10.3%)
7 (12.6%)
8 (11.5%)
DSIF-EC5
67,969 particles
3.8 Å
Closed
134,833 particles
3.4 Å
Intermediate
299,491 particles
3.6 Å
Open
224,958 particles
3.4 Å
EC mask, T=100 (very high weight on data)
1 (9.4%)
2 (6.2%)
3 (12.1%)
4 (12.2%)
5 (19.9%)
6 (13.3%)
7 (14.2%)
8 (12.6%)
Pol II stalk mask
1 (20.4%)
2 (10.5%)
3 (9.3%)
4 (16.0%)
5 (8.2%)
6 (6.5%)
7 (11.7%)
8 (17.3%)
136,139 particles
3.6 Å
69,305 particles
3.8 Å
106,779 particles
3.6 Å
114,533 particles, 3.6 Å
131,703 particles, 3.6 Å
Upstream DNA mask
1 (14.7%)
2 (9.8%)
3 (17.2%)
4 (19.7%)
5 (9.1%)
6 (8.3%)
7 (9.3%)
8 (11.9%)
Downstream DNA mask
1 (48.1%)
2 (21.6%)
3 (6.9%)
4 (11.8%)
5 (11.6%)
187,614 particles, 3.4 Å
81,169 particles, 3.4 Å

Supplementary Figure 1

Cryo-EM analysis of the Pol II–DSIF EC.

(**a**) SDS-PAGE analysis of the Pol II-DSIF-NELF EC after size exclusion chromatography. (**b**) Representative micrograph at −1.6 μm defocus. Scale bar, 100 nm. (**c**) Representative 2D classes from unsupervised classification. (**d**) Processing tree indicating 3D classification steps used to generate reconstructions with improved density for different DSIF domains. Densities from focused classifications are shown over a gray outline of the Pol II surface to provide context. Particle classes shown over a colored background were subjected to 3D refinement. Refined densities are shown next to the respective 3D classification. Coloring is as follows: DNA, blue; RPB4-RPB7 stalk domain, dark gray; RNA, red; DSIF domains as in Fig. 1.

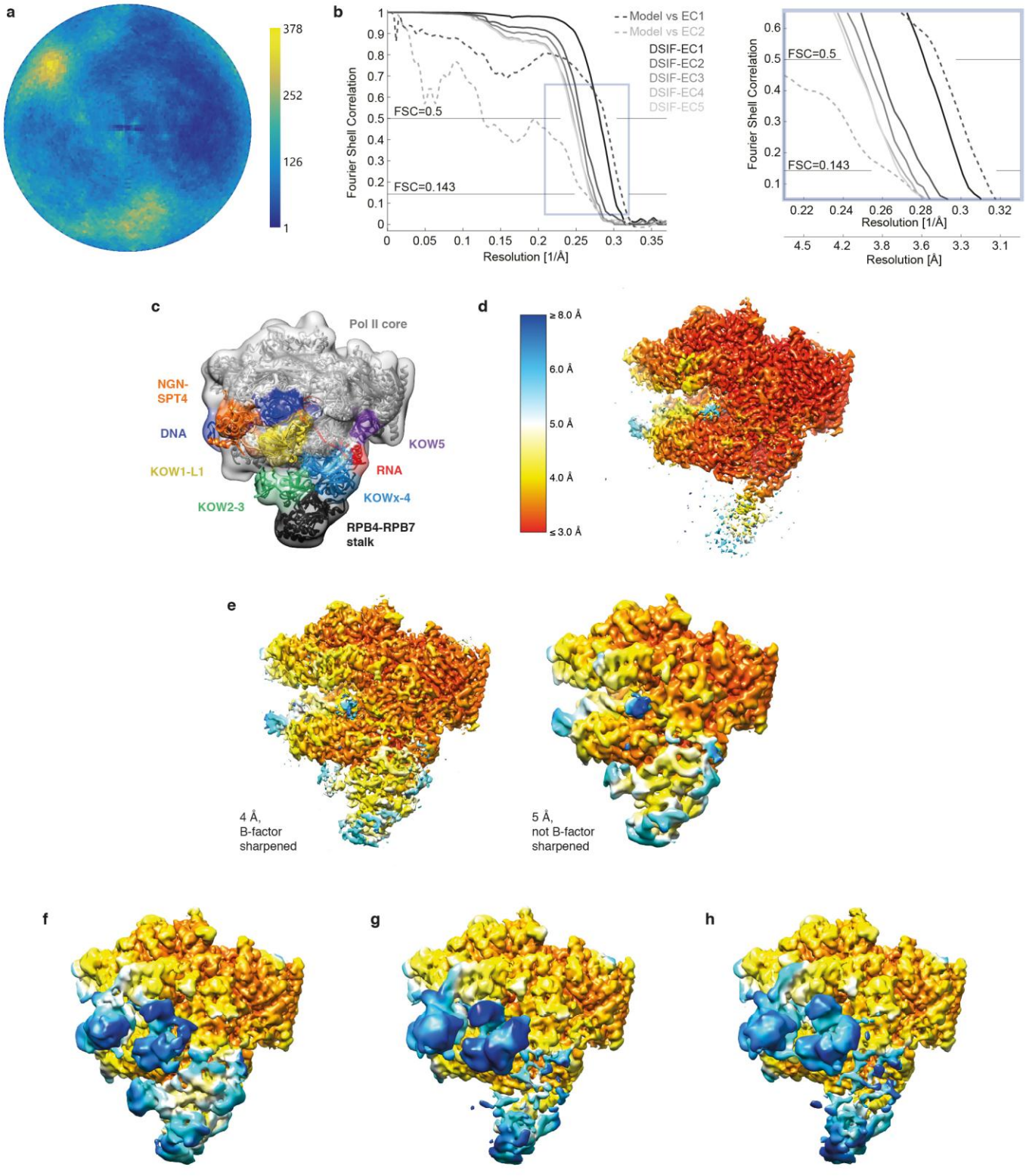

Supplementary Figure 2

Cryo-EM reconstruction statistics.

Angular distribution plot for the DSIF-EC1 reconstruction. Color scale indicates number of particles matching a particular view. (**b**) Fourier shell correlation plots for the five DSIF-EC maps described in Table S1, as well as the model versus map correlations for the selected regions of the model and DSIF-EC1 or DSIF-EC2 densities (Methods). Magnified view to the right. (**c**) DSIF-EC1 map filtered to 15 Å with domains colored as in Fig. 1. Density for all DSIF domains that fold along the EC are visible at low resolution. (**d-h**) Local resolution estimates for the five DSIF-EC maps described in Table S1. All maps are shown in a top view. (**d**) DSIF-EC1, filtered to the nominal resolution of 3.4 Å and B-factor sharpened. (**e**) DSIF-EC2 shown filtered to 4 Å and B-factor sharpened, and a second time filtered to 5 Å to allow visualization of lower resolution domains. (**f**) DSIF-EC3, (**g**) DSIF-EC4, and (**h**) DSIF-EC5 filtered by local resolution.

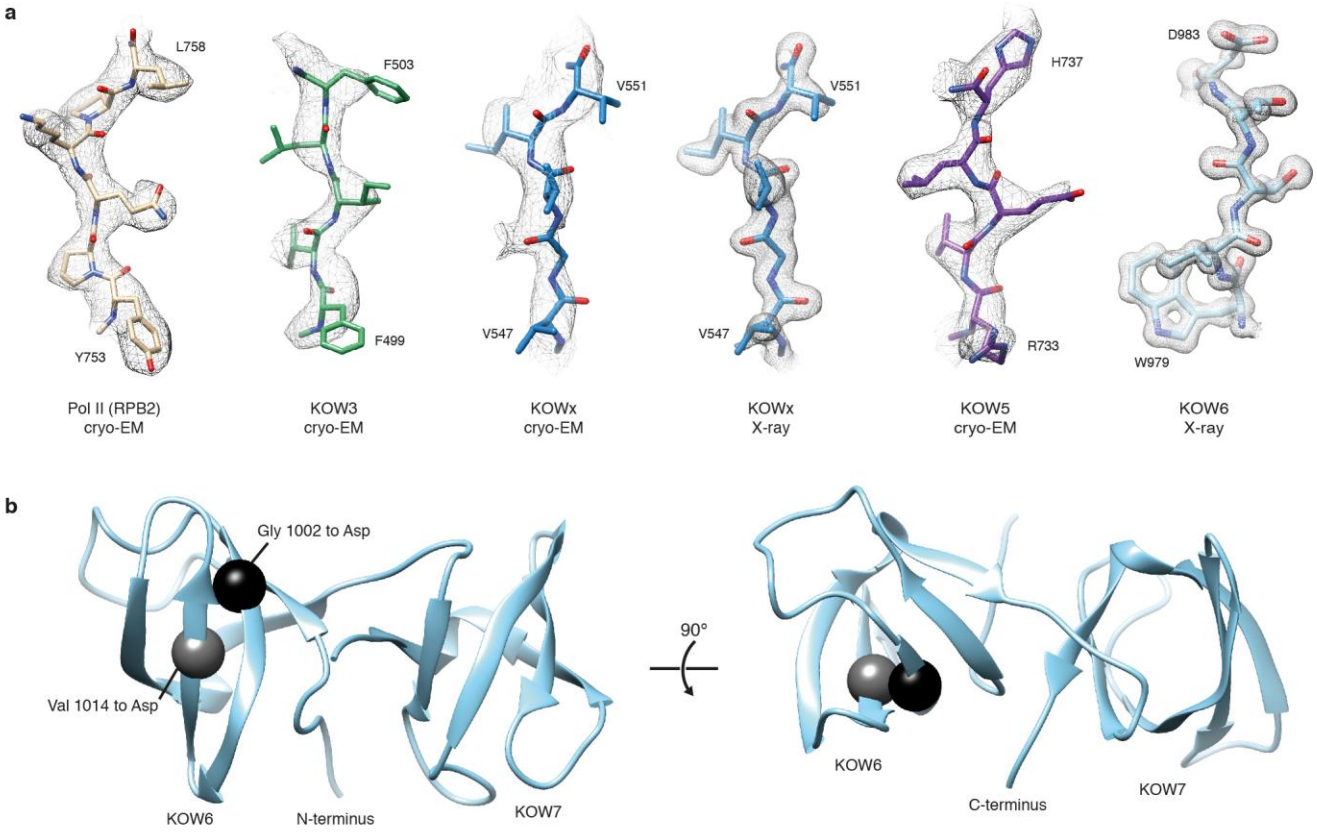

Supplementary Figure 3

Cryo-EM and X-ray modeling and density fit of the Pol II–DSIF EC and the KOW6–7 domain.

(**a**) Density overlays of representative regions within the Pol II-DSIF EC and X-ray structures. RPB2 and KOW5, DSIF-EC1 map (3.4 Å); KOW3 and KOWx, DSIF-EC2 map (4 Å), KOWx-4 and KOW6-7, experimental density maps from SAD phasing in SHELX. (**b**) Two views of the KOW6-7 crystal structure with mutations leading to developmental defects shown as spheres; black, mutation identified in *D. melanogaster*; gray, mutation identified in *D. rerio*.

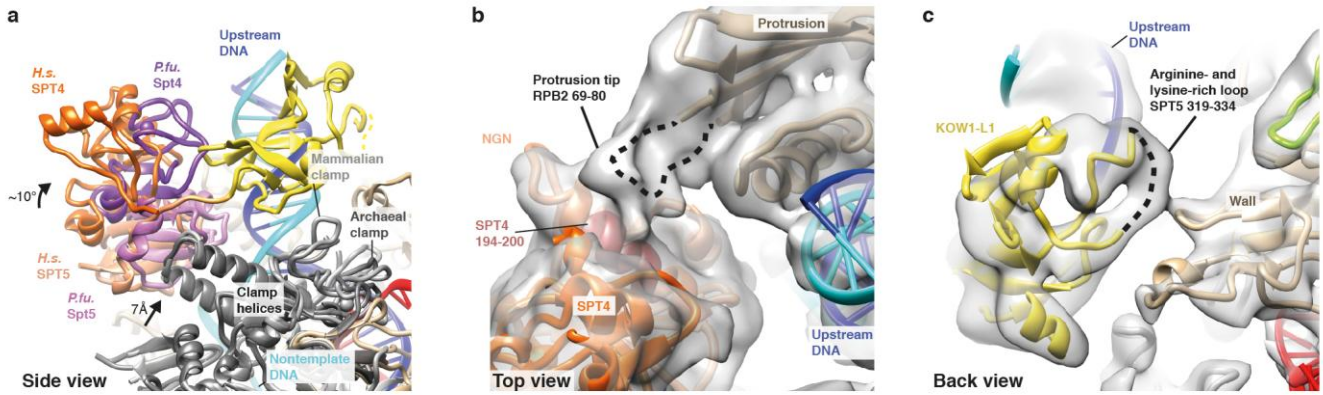

Supplementary Figure 4

Details of the DSIF DNA clamp.

(**a**) Comparison of the mammalian DSIF-EC with the archaeal (*P. furiosus*) clamp domain-NGN-Spt4 X-ray structure (PDB 3QQC)[23]. The archaeal clamp domain (dark gray) was superimposed on the mammalian clamp domain (light gray). Human DSIF coloring is as in Fig. 1. Archaeal Spt5 and Spt4 are shown in light and dark purple, respectively. The archaeal structure is shown as semi-transparent ribbon. Relative shift and rotation of the archaeal NGN-Spt4 is indicated. (**b**) Zoomed-in top view showing the density for the unmodeled RPB2 protrusion tip, which contacts helix α1 of the NGN domain. (**c**) Zoomed-in back view showing the density for the positively charged linker within the KOW1-L1 domain that contacts the RPB2 wall.

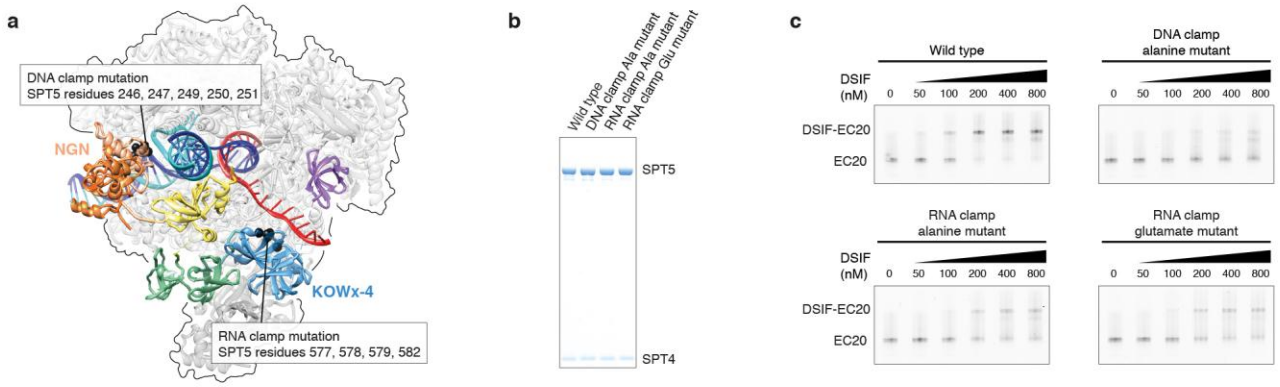

Supplementary Figure 5

Mutations in DSIF regions that contact nucleic acids are important for the binding of DSIF to the Pol II EC.

(**a**) Location of the mutated sites in DSIF shown as black spheres on the Pol II-DSIF EC structure colored as in Fig. 1. (**b**) SDS-PAGE analysis of equimolar amounts of purified DSIF mutants. (**c**) EMSA of EC20 with DSIF and the indicated mutant forms of DSIF. Elongation complexes were formed in vitro using a DNA-RNA bubble scaffold containing 20 nucleotides of 5'-FAM-labeled RNA (EC20) (Methods). RNA concentrations were 100 nM. Image was cropped to show only relevant areas.